

AD-A139 198

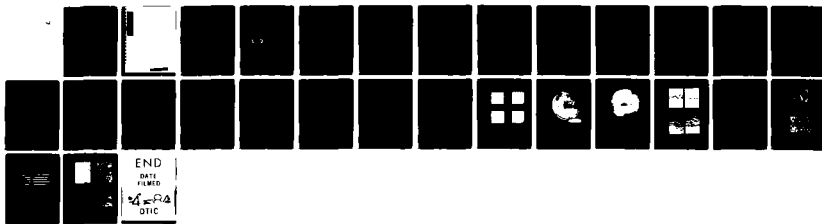
APPLICATION OF RAPIDLY SOLIDIFIED SUPERALLOYS(U) PRATT  
AND WHITNEY AIRCRAFT GROUP WEST PALM BEACH FL A R COX  
AUG 76 PWA-FR-7839 F33615-76-C-5136

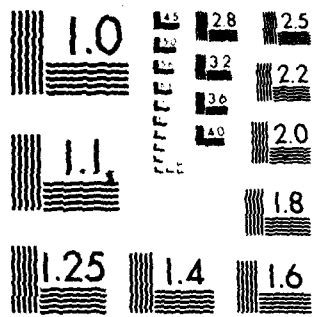
1/1

UNCLASSIFIED

F/G 11/6

NL





MICROCOPY RESOLUTION TEST CHART  
NATIONAL BUREAU OF STANDARDS-1963-A

AD A139198

84 03 20 091

**UNCLASSIFIED**

SECURITY CLASSIFICATION OF THIS PAGE (When Data Entered)

REPORT DOCUMENTATION PAGE		READ INSTRUCTIONS BEFORE COMPLETING FORM
1. REPORT NUMBER	2. GOVT ACCESSION NO. <b>AD-A139198</b>	3. RECIPIENT'S CATALOG NUMBER
4. TITLE (and Subtitle) <b>APPLICATION OF RAPIDLY SOLIDIFIED SUPERALLOYS</b>		5. TYPE OF REPORT & PERIOD COVERED <b>Quarterly Report 1 May - 31 July 1976</b>
		6. PERFORMING ORG. REPORT NUMBER <b>FR-7839</b>
7. AUTHOR(s) <b>A. R. Cox</b>		8. CONTRACT OR GRANT NUMBER(s) <b>F33615-76-C-5136</b>
9. PERFORMING ORGANIZATION NAME AND ADDRESS <b>United Technologies Corporation Pratt &amp; Whitney Aircraft Group Box 2691, West Palm Beach, Florida 33402</b>		10. PROGRAM ELEMENT, PROJECT, TASK AREA & WORK UNIT NUMBERS
11. CONTROLLING OFFICE NAME AND ADDRESS <b>Defense Advanced Research Projects Agency 1400 Wilson Boulevard Arlington, Virginia 22209</b>		12. REPORT DATE <b>August 1976</b>
		13. NUMBER OF PAGES <b>27</b>
14. MONITORING AGENCY NAME & ADDRESS (if different from Controlling Office) <b>Air Force Materials Laboratories Wright-Patterson AFB, Ohio 45433</b>		15. SECURITY CLASS. (of this report) <b>Unclassified</b>
		15a. DECLASSIFICATION/DOWNGRADING SCHEDULE
16. DISTRIBUTION STATEMENT (of this Report)  <b>Approved for Public Release, Distribution Unlimited</b>		
17. DISTRIBUTION STATEMENT (of the abstract entered in Block 20, if different from Report)		
18. SUPPLEMENTARY NOTES		
19. KEY WORDS (Continue on reverse side if necessary and identify by block number) <b>Superalloys, Powder Metallurgy, Rapid Solidification, Turbine Airfoils, Centrifugal Atomization, Convective Cooling</b>		
20. ABSTRACT (Continue on reverse side if necessary and identify by block number)  <b>This program is being conducted for the purpose of applying the principle of fast solidification to superalloy powders and subsequent development of stronger compositions for jet engine turbine airfoils. Centrifugal atomization and forced convective cooling of the material are being used for producing the fast cooled material. During this report period, high speed operation of the atomizer was achieved with resultant high yields of superalloy powder. Metallographic evaluation</b>		

UNCLASSIFIED

SECURITY CLASSIFICATION OF THIS PAGE(When Data Entered)

continued to show cooling rates in excess of  $10^5$  °C/sec and also showed the existence of a "microcrystalline" structure in the rapidly quenched powder, as opposed to the classically dendritic form. This crystallite form appears as a more homogeneous structure with almost complete, if not total, secondary phase suppression within the crystallites. Four experimental lots of material were compacted and extruded for initiation of the heat treat and mechanical test program. The working operations proceeded without difficulty.

**S** DTIC  
ELECTE **D**  
MAR 20 1984  
B

Accession For	
NTIS GRA&I	<input checked="" type="checkbox"/>
DTIC TAB	<input type="checkbox"/>
Unannounced	<input type="checkbox"/>
Justification	
By _____	
Distribution/	
Availability Codes	
Dist	Avail and/or Special
A-1	

DTIC  
COPY

UNCLASSIFIED

SECURITY CLASSIFICATION OF THIS PAGE(When Data Entered)

109000

## SUMMARY

This program is being conducted for the purpose of applying the principle of fast solidification to superalloy powders and subsequent development of stronger compositions for jet engine turbine airfoils. Centrifugal atomization and forced convective cooling of the material are being used for producing the fast cooled material. During this report period, high speed operation of the atomizer was achieved with resultant high yields of superalloy powder. Metallographic evaluation continued to show cooling rates in excess of  $10^5$  °C/sec and also showed the existence of a "microcrystalline" structure in the rapidly quenched powder, as opposed to the classically dendritic form. This crystallite form appears as a more homogeneous structure with almost complete, if not total, secondary phase suppression within the crystallites. Four experimental lots of material were compacted and extruded for initiation of the heat treat and mechanical test program. The working operations proceeded without difficulty.

CONTENTS

SECTION		PAGE
	ILLUSTRATIONS . . . . .	4
I	INTRODUCTION . . . . .	5
II	PROCESS MECHANICS . . . . .	7
III	MATERIAL EVALUATION . . . . .	18

## ILLUSTRATIONS

FIGURE		PAGE
1	Experimental Powder Rig . . . . .	7
2	Speed Influence on IN100 Particle Size Distribution . . . . .	10
3	Particle Size Distribution at 98.5 m/sec Velocity . . . . .	10
4	Predicted Speed to Attain Given Particle Size in IN100 Alloy . . . . .	11
5	Observed Speed Characteristics on IN100 Particle Size . . .	12
6	Swirl Nozzle Effect on Gas Partitioning . . . . .	16
7	IN100 Powder Microstructures . . . . .	19
8	Dendritic Appearance in IN100 Alloy Powder . . . . .	20
9	Microcrystalline Structure Observed in IN100 Powder . . . .	21
10	Ti and Cr Probe Trace Across IN100 Dendrites . . . . .	22
11	Ti and Cr Probe Trace Across IN100 Microcrystal . . . . .	22
12	Appearance of Compacted Billets . . . . .	24
13	Microstructure After 1850°F Compaction . . . . .	24
14	As Extruded IN100 Billet . . . . .	25
15	Microstructure of Extruded IN100 . . . . .	26

## SECTION I

### INTRODUCTION

The performance improvements of today's military gas turbine, such as the Pratt & Whitney Aircraft F100, over earlier engines were made possible through advancements in design technology and materials processing. Better alloys, by virtue of chemical composition, played only a minor role in achieving present day capability. Future engine projections, however, are demanding that better materials be developed in order that still higher levels of performance can be achieved.

The turbine module is especially dependent on improvement in alloy properties such as higher temperature capability, better stability, and better corrosion resistance. The alloys presently being used in this section were developed more than 15 years ago. It has not been that a lack of development interest has existed since then that these alloys are still in use. Rather, it has been the inability to improve the nature of alloying under conditions now imposed for subsequent processing and component fabrication. Precision casting alloy compositions are limited because of such constraints as crucible and mold interactions and massive phase occurrence. Forging alloys are limited because of constraints of segregation during ingot processing.

Superalloy powder metallurgy studies conducted at the P&WA/Florida facility have shown that the use of powder, particularly powder solidified at very high rates of cooling, can eliminate the constraints noted and can enable more effective alloying for the improvement of basic material properties. Several examples which support this statement are as follows. Chemical segregation in fast cooled superalloy powders can be controlled to a submicron level. Massive phases can be eliminated. Solubility of alloying elements can be extended without deleterious phase reaction. None of these can be achieved in ingot or precision casting.

Further, the inherent homogeneity of the powder is such that subsequent processing and heat treatment can be used very effectively to promote maximum material utilization. Abnormal grain growth, for example, can be achieved in superalloy powder materials for optimization of mechanical properties above  $1/2 T_M$ . MAR M-200 alloy powder, processed and reacted in this manner, is, in fact, stronger than and as ductile as the same composition cast in a directional mode.

P&WA/Florida has constructed a device that can produce metal powders solidified and cooled at rates in excess of  $10^5$ °C/sec. The underlying principle is forced convective cooling, whereby powder particles of controlled size are accelerated into a high thermal conductivity gaseous medium maintained at high  $\Delta T$  between itself and the metal particle.

The purpose of this ARPA sponsored program is to refine the process mechanics used with the powder producing device for fast quenching bulk lots of powder and, subsequently, apply the technology of rapid solidification to the development of an alloy composition that is stronger than the existing MAR M-200 alloy and that can be implemented for the production of better turbine airfoils.

The program is a 40-month effort and is organized as a progression of events starting with a parametric study of the requirements necessary to achieve high yields of fast quenched powder and terminating in the fabrication and testing of turbine airfoils. This report is the second technical report and covers the 3rd - 6th month of the program. It deals with the study of producing fast quenched powder and includes observations on resulting material characteristics.

SECTION II  
PROCESS MECHANICS

The device which is being used for production of fast cooled powder is one in which a central rotary atomizer disintegrates a molten metal stream into fine particles and accelerates them into a high mass flow helium quench environment. The unit is illustrated in Figure 1 and principal design parameters are based on a metal atomization rate of 0.15 kg/sec. It is presently capable of handling metal charges up to 23 kilograms (based on nickel). The unit has 3 annular gas nozzles which are sized to gas mass flow and velocity commensurate with maintenance of a high  $\Delta T$  on the basis of calculated heat flux profiles and particle trajectories. For 0.15 kg/sec metal flowrate, the gas requirement translates to  $\sim 0.75$  kg/sec. A radial impulse turbine is used for the atomizer drive. The unit is provided with conventional vacuum induction melting and tundish metering. The sequence of operations includes vacuum melting, He backfilling, pouring and atomization, and finally gas quenching.

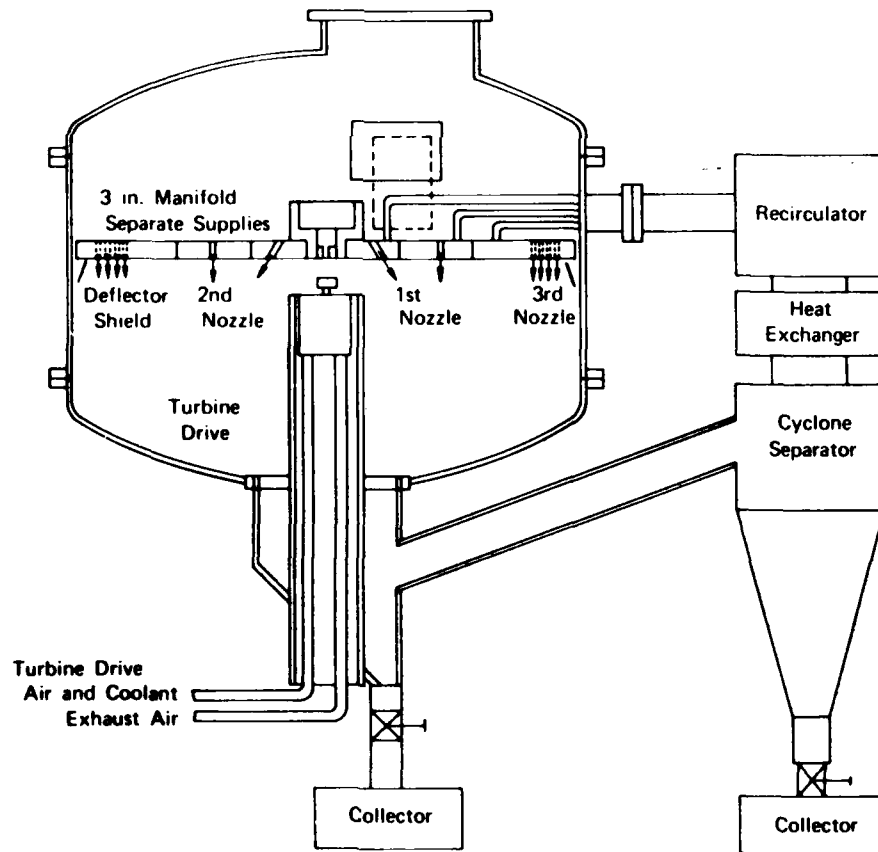


Figure 1. Experimental Powder Rig

FD 90727A

In the previous report period, the bulk of activity was expended on relating the steady-state operation of the atomizer and interactions of the powder generator with the pouring and quenching mechanisms. During that time, it was found that molten stream stability was essential to effective atomization. Additionally, it was found that a local heat balance on the atomizer was required in order to achieve steady-state operation and control of particle generation. Atomizer speed was a problem in the form of both maximum speed attainable and speed decay during running. The balance of operations appeared acceptable for that time in the program.

The effort expended during this report period was directed toward improving the atomization process by modifying the turbine drive and in establishing reasonable control limits for the balance of operations such that high quality product could be obtained from the operation. Eighteen runs were made during this period for this purpose. All runs were made with IN100 alloy which was procured as a single master heat, vacuum induction melted and vacuum arc remelted. The nominal composition of this material was 12.5% Cr, 4.5% Ti, 0.7% V, 18.0% Co, 0.06% Zr, 0.06% C, 4.8% Al, 3.5% Mo, 0.015% B, balance Ni.

The sequence of operations in producing the powder from the experimental rig is as follows:

- Melting
- Pouring
- Atomization
- Quenching
- Collection.

The following paragraphs describe the influence of each as observed during the past 18 runs.

#### Melting

With the exception of modifications to the rig made in order to improve the vacuum environment, no changes to the melting cycle were made from that previously reported. In the initial work, the attainable vacuum level was considered too high (i. e.,  $40\mu$ ), as was the rate of rise. The cause was attributed to a faulty O-ring seal plate on the turbine drive assembly. The plate assembly was redesigned to assure positive sealing, and installed prior to the first run of this period. It has worked successfully from its time of installation. Vacuum levels now being maintained are on the order of  $5-15\mu$ , with rates of rise less than  $10\mu/\text{minute}$ . These levels have proven to be entirely satisfactory from a quality point of view, as discussed in Section III.

#### Pouring

No changes to the pouring system were made during this period. We are continuing to use tundish metering with manual liquid head control and nozzles sized to deliver about 0.15 kg/sec. Transients at the beginning and ending of each run are minimal, on the order of several seconds each, and do not impose any difficulty in setting-up controlled skulls on the atomizer itself. Erosion characteristics are checked after each run and in conjunction with analyses of the powder itself. No conditions judged unsatisfactory have been detected for the flow rate and flow times used to date.

## Atomization

The major thrust during this report period was to improve the operation of the atomizer in order to attain higher yields of powder capable of being quenched at the rates desired. In the previous report period, speeds were limited to about 16,000 rpm and, during operation, would decay to about 10,000-12,000 rpm. The cause for this was due basically to ineffective lubrication of the bearings which, at that time, was being accomplished through the use of an oil mist system. The assembly was reworked during this period to incorporate a direct oil injection system and this fix has proven to be entirely satisfactory. Also, in conjunction with this rework, an additional modification was made to the turbine air supply in order to assure maintenance of speed once liquid metal pouring was started. With these modifications made, atomizer speeds on the order of 24,000 rpm are now possible, speed decay has been eliminated, and response times on the order of a fraction of a second are typical.

The first 14 runs of this period were made in order to establish a baseline with respect to rotational speed and powder yield, heat balances, repeatability, and system degradation. Of these 14, 4 were aborted because of equipment malfunctions. The balance of runs, however, ran well. Two speed conditions were selected for evaluation, one at 21,000 rpm, and the other at 24,000 rpm. These conditions correspond to tangential velocities of 84.5 m/sec and 96.6 m/sec, respectively. All runs were made using water cooled copper disks, insulated to assure that total superheat was not lost to the water.

Although readily recognizable in hindsight, the first runs of this series showed that the heat balances achieved for the low speed operations (14,000-10,000 rpm) were inadequate for the higher speeds, obviously due to the reduced dwell time of the liquid metal on the disk surface. As best as could be analyzed from high speed cinematography, the liquid metal dwell time was cut from a period on the order of 80 milliseconds to one less than 10 milliseconds. Changes to the insulation characteristics of the disk were easy enough to make, and, subsequently, operations proceeded smoothly.

The yields of powder were high for both speeds investigated. Little or no splashing occurred during startup or shutdown, and stability of operation was achieved after about 3 seconds into the run. Figure 2 shows an accumulated weight-particle size relationship for the speeds investigated. Included is a curve depicting the typical result from earlier work where transient speed conditions were constantly taking place. A log normal distribution plot is also included for  $d = 60 \mu$ ,  $\sigma = 20 \mu$ , simply for comparison purposes.

With the exception of the high end of the curves, log normal distribution shows a reasonable resemblance to the experimental data. This high end variation is attributed to startup and would have been a negligible factor had duration of running been for extended periods rather than the 60-90 second circumstance which is now used. Typical distribution according to weight retained by individually sized screens is shown in Figure 3 for one of the 96.6 m/sec runs. The appearance of log normal is evident again; however, lack of data at the low end is cause for question. It is expected that during the next several reporting periods, this information will be obtained.

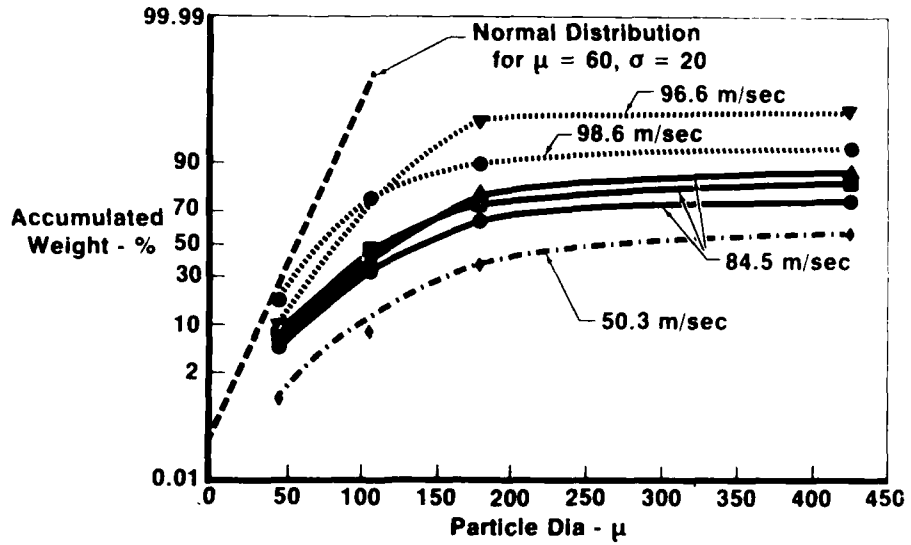


Figure 2. Speed Influence on IN100 Particle Size Distribution

FD 99965

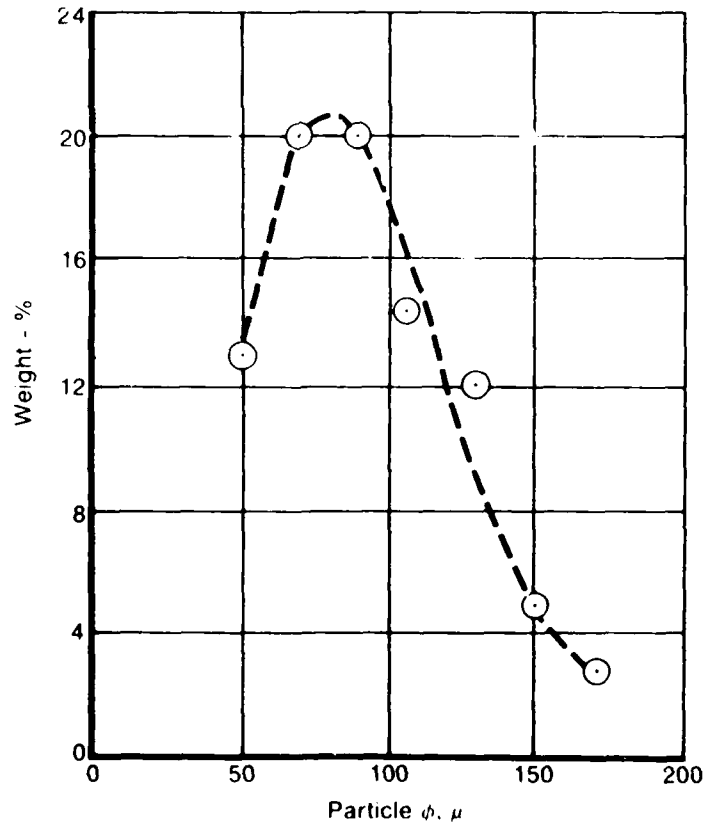


Figure 3. Particle Size Distribution at 98.5 m/sec Velocity

FD 101851

Of especial interest with respect to particle size and yields obtained is what might be an apparently significant deviation from the empirical relationship thought to hold true for rotating atomizers of the type being used in this program. The relationship in question is of the form

$$d_{sv} = K \left( \frac{\dot{M}^{0.2}}{r^{0.3} \omega^{0.6}} \right) \left( \frac{\sigma^{0.1} \mu^{0.2}}{\rho^{0.5}} \right)$$

which was described in the first quarterly report of this program and which is diagrammed in Figure 4. This relationship assumes that a ligament formation takes place prior to formation of individual droplets. If one were to discount the particle diameter-speed relationship of earlier runs because of transients, splashing, etc., and use only data obtained from runs exhibiting total stability, then a distinct departure from earlier predictions rises.

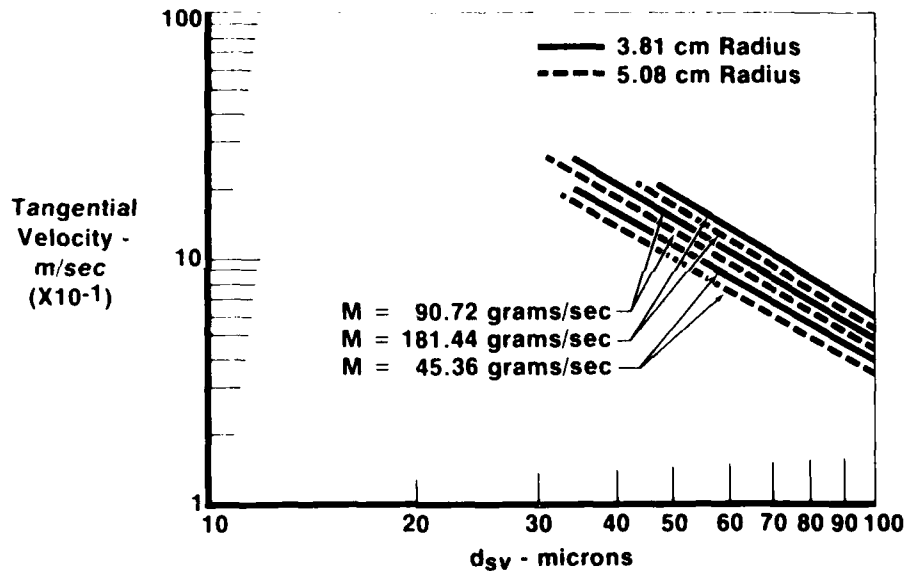


Figure 4. Predicted Speed to Attain Given Particle Size in IN100 Alloy FD 98316

In analyzing results in this light, the data might appear similar to that plotted in Figure 5. Although we measure  $d_{wt}$ , rather than  $d_{sv}$ , one can assume a constant multiplier would exist and result in parallel curves, since  $d_{sv}$ , (the surface to unit volume drop diameter) can be related to  $d_{wt}$  (the geometric weight average particle size) under conditions of a linear logarithmic probability drop size distribution.

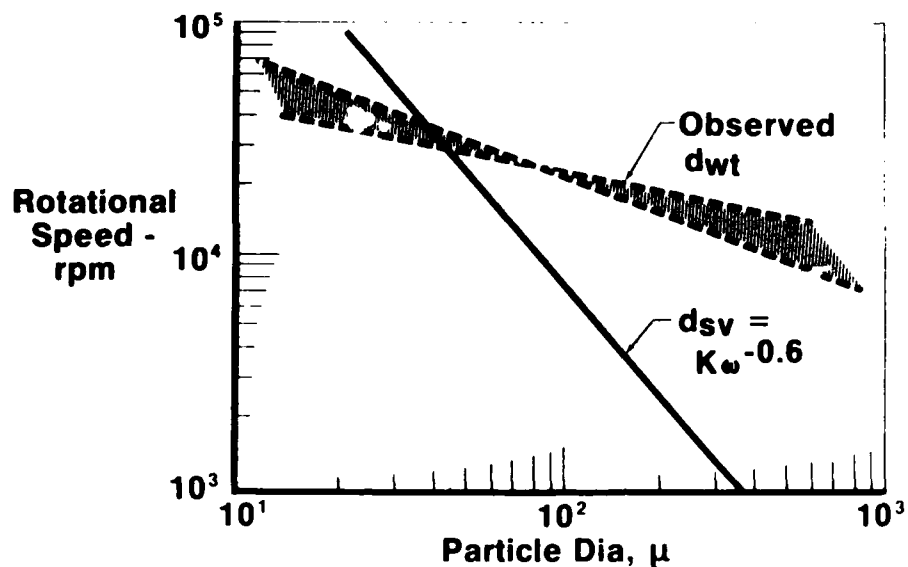


Figure 5. Observed Speed Characteristics on IN100 FD 99966 Particle Size

For the higher speeds as shown in Figure 2, this appears to be the case and the relationship between the 2 particle types can be expressed as

$$\log d_{wt} = \log d_{sv} + 1.1513 \log^2 a$$

where  $a$  is the log geometric standard deviation of the particle size. This deviation is defined as the ratio of the 84.13% size to the 50% size or the ratio of the 50% size to the 15.87% size, taken to give a number greater than 1. For those observations made to date, this relationship reduces to

$$\frac{d_{wt}}{d_{sv}} = 1.17.$$

Clearly then, this would indicate a change in exponents since the slope of  $d_{wt}$  vs speed in Figure 5 is obviously different from that of  $d_{sv}$ . If we presume that the original equation is correct for all terms and exponents except  $\omega$ , then an equation of the form

$$d_{sv} = \frac{a}{\omega^x}$$

results, where  $a$  is presumed constant (constant radius, fluid pour rate, density, etc.). Knowing that one can go from  $d_{sv}$  to  $d_{wt}$  by a constant multiplier, ( $\beta$ ), then the equation would take the form

$$d_{wt} = \beta d_{sv} = \frac{\beta a}{\omega^x} = \frac{\gamma}{\omega^x}$$

Taking the lower slope limit on Figure 5, one obtains  $600 \mu$  (wt) at 15,000 rpm and  $16.5 \mu$  at 35,000 rpm. Thus,

$$600 = \frac{\gamma}{\left(\frac{15,000\pi}{30}\right)^{x_1}} \quad \text{and}$$

$$16.5 = \frac{\gamma}{\left(\frac{35,000\pi}{30}\right)^{x_2}} .$$

Assuming the exponent is constant,  $x_1 = x_2 = x$  and

$$\frac{600}{16.5} = \left(\frac{3500}{1500}\right)^x ,$$

then the solution is  $x = 4.24$ . Similarly for the high slope limit, one obtains  $x = 2.11$ . Hence, for our present data, it would seem that  $\omega^{2.11} \leq \omega^x \leq \omega^{4.24}$ , a significant deviation from the originally thought  $\omega^{0.6}$ .

In analyzing further, though, the conditions to test for intersection of the 2 curves ( $d_{sv}$ ,  $d_{wt}$ ), a form of the type

$$d_{wt} = \beta d_{sv} = \beta \frac{C}{\omega^x}$$

where

$$C = \left(\frac{\dot{K}M^{0.2}}{r^{0.3}}\right) \left(\frac{\rho^{0.1} \mu^{0.2}}{\rho^{0.5}}\right)$$

was presumed constant for the runs of interest.

Taking logs of both sides yields

$$\log d_{wt} = \log \beta + \log C - x \log \omega ,$$

while the original equation would yield

$$\log d_{sv} = \log C - 0.6 \log \omega .$$

Thus,

$$\log d_{wt} - \log d_{sv} = \log \beta - (x-0.6) \log \omega .$$

Obviously, the curves intersect under the circumstance of

$$\frac{\log \beta}{(x-0.6)} = \log \omega .$$

If the exponent on  $\omega$  should be between 2.11 and 4.24, and if the balance of the original relationship is correct for our operation then, using common logs,  $\beta < 10$ . Therefore  $0 < \log \beta < 1$  and thus  $\log \omega < 1$ . This implies that the intersection should be at  $\omega < 10$  rpm (if  $\omega$  in the equation is expressed in rpm).

The apparent intersection, however, seems to be near 27,000-32,000 rpm. To obtain an intersection at  $\omega < 10$  rpm would require  $d_{wt} > 10^9 \mu$ , a totally unreasonable value from our work to date.

This analytical treatment suggests that the basic form of equation may not be valid for the range of speeds considered in this present effort and that, in fact, ligament mode operation may not be the principal means for particle formation. Direct drop formation theory, in which a liquid film is disintegrated directly into droplets, anticipates an exponent on  $\omega$  on the order of 1, still below the values calculated. Thus, it could be that some circumstance of "brute force" could be giving rise to the observed variations.

Interestingly, there could exist domains for which, depending on speed, control of droplet formation and size could be passed from one predominant factor to another. For example, as disk rpm goes to zero, the physical properties of the material, and the use of a disk of specific size and a stream of certain diameter and velocity suggest that there would be some "largest size" particle possible, meeting the various physical conditions of the system. As the disk rpm is increased from zero, the particle size produced would drop rapidly as a function of rpm, then settle down to some predictable function of the rpm.

In considering the opposite extreme, the case of infinite rpm, a mean size of zero is physically unacceptable. This suggests an asymptotic approach to zero with increasing rpm.

The "center region" of operation is left unaccounted for, then, which could well vary from a few hundred rpm to perhaps several tens of thousands of rpm.

Several modes of particle production are well known and, for each mode, mean and/or maximum particle sizes have been suggested. Regardless, the sizes predicted all relate in some form to the angular velocity of the atomizer disk. It is, therefore, reasonable to surmise that, as the rpm is increased from zero, particle sizes drop rapidly, stabilize to some function of  $\omega$  for a range of rpm, go through a transition region to some other functional dependence on  $\omega$ , and so on, until at some high value of rpm, the dependence of  $d_{wt}$  or  $d_{gv}$  on  $\omega$  would asymptotically approach zero (or perhaps some other value; on the order of the mean free path length of the gas molecules, for example).

The effort in the next report period will be directed toward evaluation of this hypothesis, since this represents the maximum potential for cooling rate possible for a device of the type now being used. A new turbine drive assembly has been designed for operation to twice the tangential velocities now possible. With this spread in speed, it should be possible to predict with some reasonable degree of accuracy what particle sizes are possible for rotating atomizer system.

In addition to the 14 test runs for evaluation of atomization, 4 additional runs were made for product to be used subsequently for material test and evaluation. These runs were all made at 96.6 m/sec tangential velocity and all proceeded with no difficulty. Analyses of yield showed that repeatability was good and typical for that shown on Figure 2.

#### Quenching

The nozzle assemblies to deliver the He quench gas and the methods of operation were not changed with any degree of significance from the previous report period. The gas mass flow was increased from  $\sim 0.23$  kg/sec to  $\sim 0.50$  kg/sec, however, for the purpose of providing more data on gas turbulence which had been observed previously in the region surrounding the atomizer. Coupled with this change was the installation of nickel foil probes inserted at various locations around the disk periphery which would act as indicators for local disturbances in the gas stream. These foils were about 0.13 mm thick by  $\sim 1.2$  cm by  $\sim 5$  cm and were tack welded into place. From observations obtained from both the real time video system and high speed cameras, what became evident was that turbulence discernible at low disk speeds was pretty much negated at the higher speeds because of a pumping action of the atomizing process itself. This can be described in the following manner. With the gas flow on and the disk stationary, and no metal flow, a turbulent condition was observed at the disk rim. With the gas on and the disk at speed, but still no metal flow, the conditions of turbulence still existed. With the gas on, the disk at speed, and the liquid metal flowing, the turbulent features were no longer observed. How one would measure the pumping nature of the atomizing process and relate it to the gas action at the nozzles is not clear to us. It does point out, however, that a streamlined flow condition is obtained at the disk, to the extent that interference with the skull formation does not occur. This is judged an important point from an interaction point of view and in the use of shields, etc., to compensate. In the next report period, the gas flow will be taken up to 100% of design capacity for further study. Once this is done, the combined data from the maximum gas flow and the higher turbine speeds should totally define cooling rate expectations possible from a device of this type.

Substitution of a swirl nozzle, rather than the cross flow nozzle now in use, was evaluated further in this period as an alternate means for more efficient gas delivery. Previous computer modeling showed that a delivery system of this type could set up an abrupt transition from hot gas at the disk to cold gas in the quench by centrifugal force acting on the difference in density.

A 1/4 scale rig was constructed during the previous report period to verify the effectiveness of separation, using He to simulate hot gas and air to simulate cold. The degree of separation was determined by measuring  $O_2$  concentrations within the "hot region." No  $O_2$  was indicative of total separation, while 21%  $O_2$  was indicative of total displacement.

Testing was done under varying conditions of air (cold gas) flow for a constant He (hot gas) flow. The results are shown in Figure 6 and compare mix characteristics observed for both cross-flow and swirl-flow configurations. At low flow rates, the cross-flow tendency to mix is less, while at the higher flow conditions, those commensurate with rig operation, the swirl mode significantly retards this tendency.

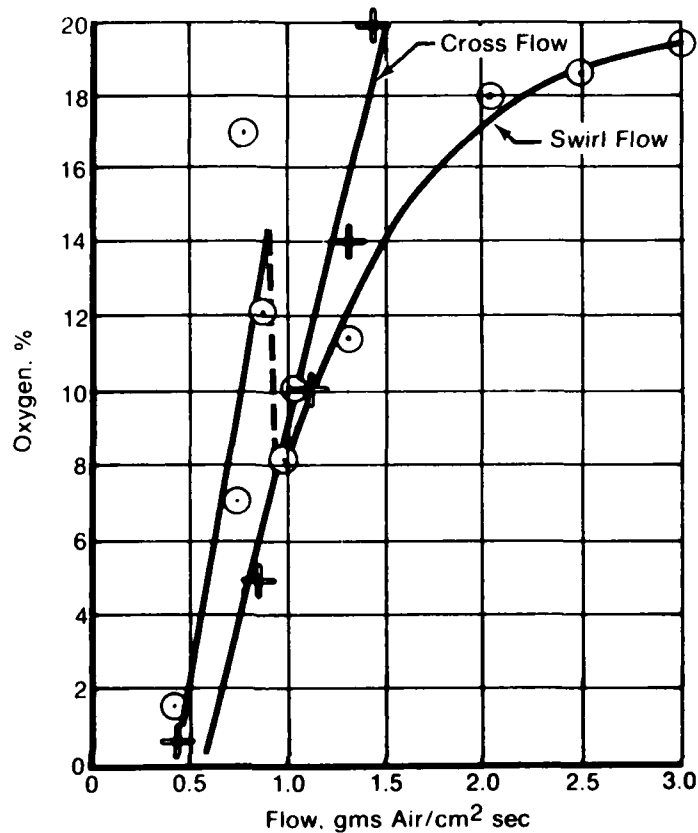


Figure 6. Swirl Nozzle Effect on Gas Partitioning FD 101852

It is thought that the tendency to mix is proportional to the shear between the hot and cold gases and the tendency to separate is proportional to the product of density difference and the centrifugal acceleration acting at the mixing zone. The results tend to confirm these beliefs in that both models, at low mass flow where shear is predominant, exhibit increasing tendency to mix. As the flow is increased, however, the cross flow mode continues to mix proportionately higher while the swirl model shows a transition to lower values, with subsequently more separation as the mass flow rises.

Further testing is planned for this unit with respect to maximizing hot-cold separation within the confines of the existing powder rig. The data is sufficiently interesting, however, to proceed with a preliminary layout for incorporation.

#### Collection

The collection system on the powder device itself has not been changed from that previously reported. Contamination via erosion in the piping or cyclone separator is still not perceptible using our available measuring standards or analytical equipment. A vacuum interlocked He dry box has been added, though, in order to inertly remove the powder product from the device into a second inert area where subsequent operations can be manually carried out. The assembly is

typical of most inert gas boxes with the exception of modifications to transfer the collectors. It is generally maintained at  $O_2$  concentrations on the order of 10-150 ppm.

An interesting point in conjunction with the transfer of powders is associated with how to store them inertly until such time that further use is desired. We found the use of home canning jars to be ideal for our purposes. They are clean, easy to work with, and can be readily evacuated to some lower than atmospheric pressure. The lid position then can be visually examined to determine whether a break to the ambient atmosphere has occurred or whether the material remains in its inert state.

### SECTION III

#### MATERIAL EVALUATION

The powdered material from each run is being evaluated with respect to cooling rates attained, effect of such rates on microstructure, and product acceptability relative to present quality standards for superalloy powder.

The typical appearance of the alloy powder was described earlier as spherical and free from aggregate formation like that which occurs when molten particles impact one another. Some flake is evident, as are fractured particles, presumably from impact with the chamber of the device. We have not quantified the extent of these occurrences at this time. The fraction is small presently and, once the gas flow is taken to 100% capacity, it should become even smaller. At that time, a quantitative undertaking will be made to define how extensive this condition is.

Microstructural study of the powders continues to show that cooling rates in excess of  $10^5$  °C/sec are obtained in the less than  $100\mu$  particles, as measured by dendrite arm spacing. However, some very interesting observations were made in this past period which, in our opinion, might be very significant with respect to the study of new alloy compositions. What is referred to in this sense is the appearance of a "microcrystalline" structure in the as-produced powder, rather than the classical dendritic pattern which had been reported previously. Typical microstructures, as they appear from present operations, are shown in Figure 7. The coarse particles continue to show a preponderance toward dendritic solidification; however, in the finer powders, a change to a "microcrystalline" state is evident. It has not been possible yet to produce an entire lot of material favoring this latter state, but it has appeared that certain run conditions favor a predominant "microcrystalline" form, while others favor the classical dendritic form. That this occurrence is not a spurious circumstance owing to methods of metallographic preparation or sampling is shown in Figures 8 and 9, which depict entire particles displaying the forms described.

The controlling factor for this change seems to be predicated upon the extent of supercooling, in that, after some critical degree of supercooling occurs, solidification changes from dendritic to microcrystalline. What particular machine parameters are most critical to this circumstance is not entirely clear. We presently measure some 35 separate functions during operation and, as one function is independently varied, it, by necessity, will cause variation to others.

The amount of superheat added to the melt is the first variable one would probably consider but, in all runs to date, the superheat condition has been held constant. Superheat remaining in the particles after atomization becomes the second factor in our opinion and machine parameters are presently being programmed to deliberately modify particle superheat to determine this influence.

What appears most interesting about this microcrystalline state is that if one measures crystallite size, and compares to secondary dendrite arm spacing in particles of equal diameter, the mean crystallite diameter invariably is larger.



~ 150 $\mu$  Particle



~ 100 $\mu$  Particles

10 $\mu$



1 $\mu$

Particle Sizes  $\leq$  65 $\mu$

Figure 7. IN100 Powder Microstructures

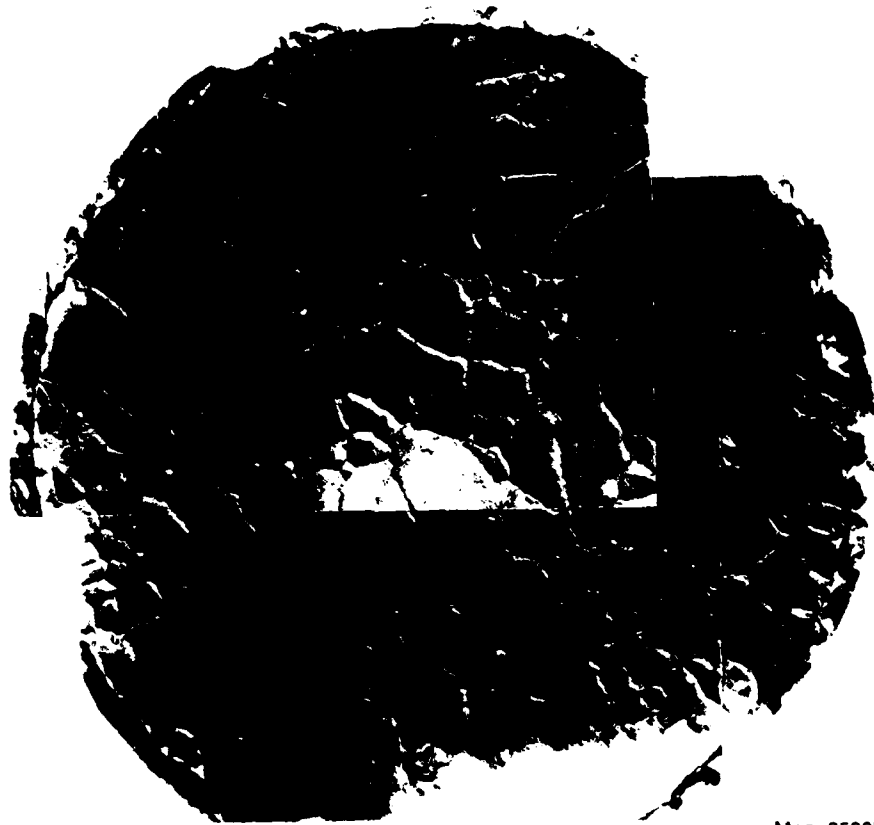
FD 101853



Mag 3590X

Figure 8. Dendritic Appearance in IN100 Alloy Powder

FD 101854



Mag: 3590X

Figure 9. Microcrystalline Structure Observed in  
IN100 Powder

FD 101855

At first, this was thought to be some condition of slower cooling for, had cooling rate been the same, our belief was that crystallite diameter and secondary arm spacing would have been equal. But in analyzing phase suppression and homogeneity of structure, the crystallites show near total secondary phase suppression and homogeneity within the crystals boundaries, whereas the dendritic structures do not. At the crystallite walls, it is apparent that solute rejection occurred during the solidification, but the extent was appreciably less than that observed in the typically dendritic structures. Figures 10 and 11 depict this variation in the form of X-ray line profiles. Our microprobe device is an Etec Autoprobe with best sensitivity occurring for titanium. Quantitative checks by point counting dendritic and microcrystalline particles of equal size showed that the maximum variation in titanium was 0.5% from microcrystal center to boundary whereas the maximum variation in the finer dendritic structure was 1.9%, an improvement of more than three-fold. This seemingly could be a major benefit to the future studies of alloying capabilities and extensive effort is planned for the next report period to determine how to repetitively force the powder into a microcrystalline mode of solidification and to what extent can benefits be derived.

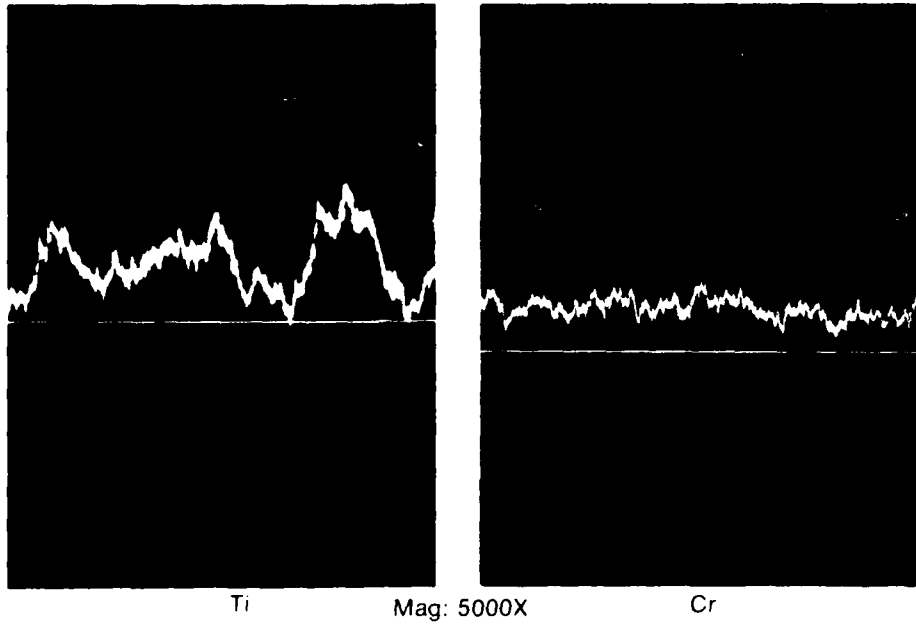


Figure 10. Ti and Cr Probe Trace Across IN100 Dendrites                      FD 101856

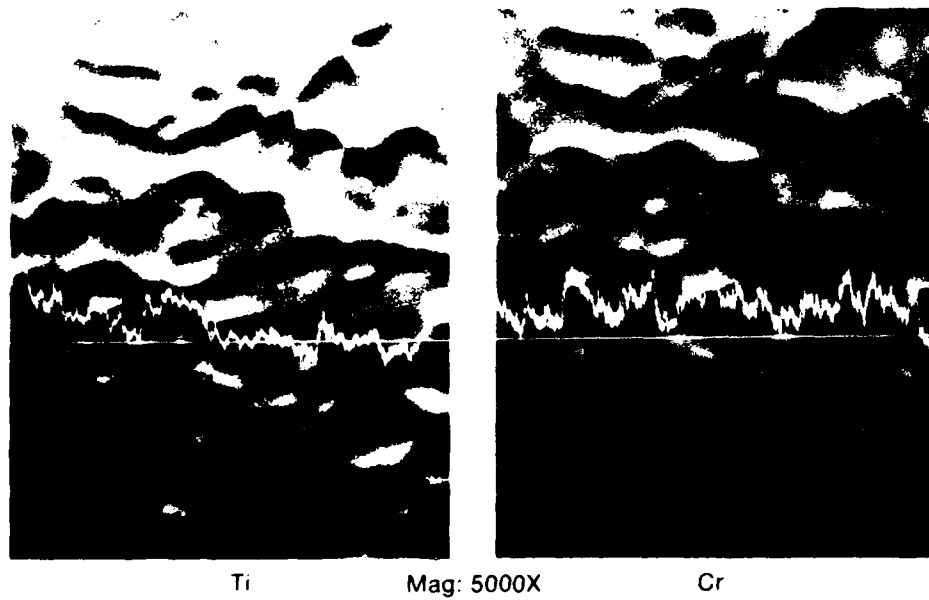


Figure 11. Ti and Cr Probe Trace Across IN100 Microcrystal                      FD 101857

With the He dry box now operative, it has been possible to accurately define quality of the powder with respect to O<sub>2</sub> pickup during processing. The starting ingot material has approximately 22-30 ppm O<sub>2</sub>. After processing into powder, typical results of the loose powders are on the order of ~70 ppm for the coarse particles (-80+140 size fraction) and ~140 ppm for the finer (-325 size fraction). These numbers appear very reasonable for loose powders and should be tempered by the recognition that He was present to some extent in the samples, which appears as O<sub>2</sub> in the thermal conductivity cell used for measurements.

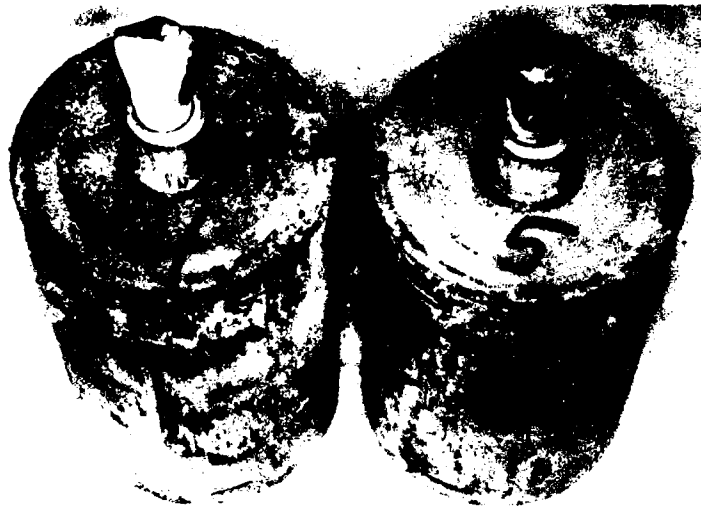
After compaction into solid bodies, the O<sub>2</sub> concentrations have been typically 50-80 ppm for all size ranges. An interesting note with respect to O<sub>2</sub> pickup occurred during one of the 24,000 rpm runs. A wire probe had been inserted to study particle trajectories during the period of atomization. It was believed that a minor portion of the powder would adhere to the wire which, subsequently, could serve as a visual aid to determine actual paths travelled. Instead, a significant portion of the powder adhered and formed a solid mass. Samples for O<sub>2</sub> were removed and results showed that no appreciable change in concentration had taken place from that measured for the starting ingot. Although this was only a single test, the data suggested that O<sub>2</sub> control will be primarily dictated by one's ability to handle the powders after atomization.

The last 4 lots of powder made during this period were compacted into billet form and subsequently extruded into barstock for test and evaluation. A control sample of conventional IN100 alloy powder was run concurrently with these 4 in order to provide a basis for comparison. All billets were ~4.5 kg samples. Compaction to 100% theoretical density was carried out at 1010°C, after canning and outgassing the powder in mild carbon steel containers. The compacted sections were recanned in stainless steel cylinders and subsequently extruded at a nominal reduction of 6 to 1 at 1065°C.

The control sample was prepared in essentially the same manner to that presently used for B/M production of powder for the F100 engine. The experimental powder samples were sized to provide 3 billets of less than 100 $\mu$  particles, and one billet of less than 65 $\mu$  particles.

The typical compaction billet appearance is shown in Figure 12. Each is approximately 15 cm long by 7-1/2 cm diameter. The microstructure of the -65 $\mu$  compaction is shown in Figure 13 and is fairly representative of the other 4. Full density was achieved and bonding appeared good. Recrystallization was very limited.

The extruded forms are shown in Figure 14 and the microstructures are shown in Figure 15. The barstock is sound and has no noticeable extrusion defects. Recrystallization is not complete and suggests a need for higher reductions and/or extrusion temperature. At this time of writing, the material is being sectioned for chemical and metallographic evaluation, heat treat studies, and mechanical property testing. Results of this effort will be made available in the next quarterly report.

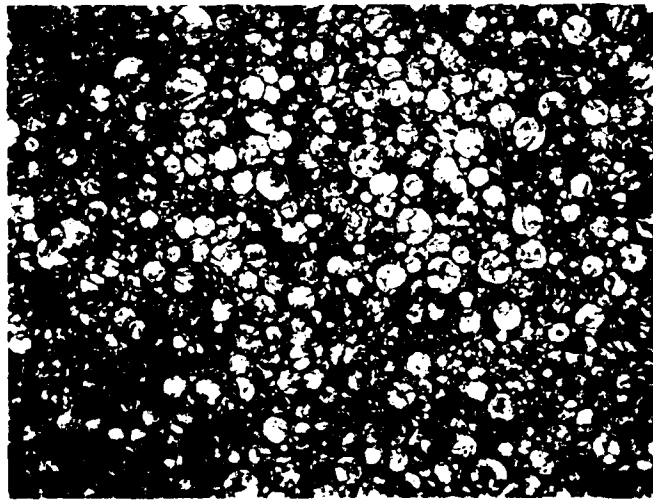


Mag: About 1/2X

FAL 38940

Figure 12. Appearance of Compacted Billets

FD 101867



Mag: 100X

-65 $\mu$

Replicated Surface

Figure 13. Microstructure After 1850°F Compaction

FD 101908

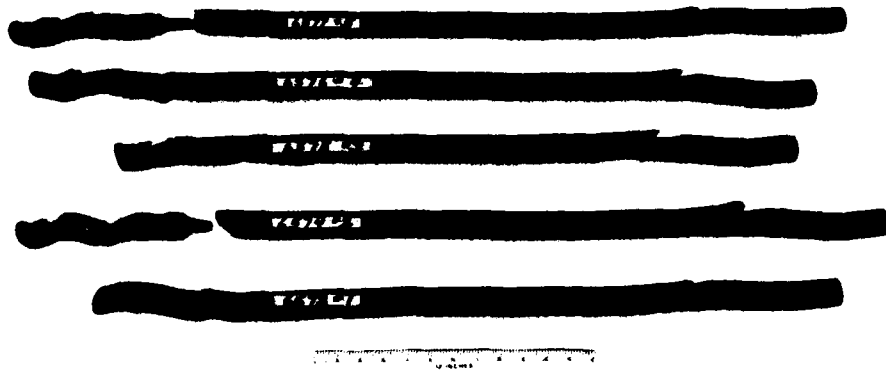
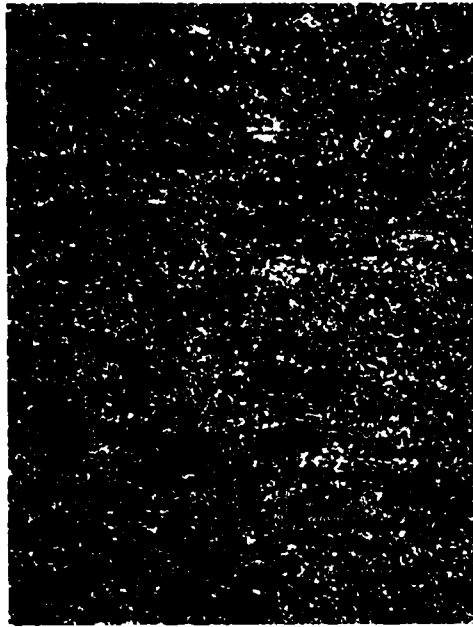


Figure 14. As Extruded IN100 Billet



Long



Trans

-65 $\mu$



Long



Trans

Mag: 100X

-140 $\mu$

Figure 15. Microstructure of Extruded IN100

FD 101858